Prepared for submission to JHEP

Charged Higgs Search via $AW^{\pm}/HW^{\pm}$ Channel

Baradhwaj Coleppa, Felix Kling, Shufang Su

Department of Physics, University of Arizona, Tucson, AZ 85721, USA

E-mail: baradhwa@email.arizona.edu, kling@email.arizona.edu, shufang@email.arizona.edu

Abstract: Models of electroweak symmetry breaking with extended Higgs sectors are theoretically well motivated. In this study, we focus on models with a low energy spectrum containing a pair of charged scalars $H^{\pm}$, as well as a light scalar H and/or a pseudoscalar A. We study the $H^{\pm}tb$ associated production with $H^{\pm} \to AW^{\pm}/HW^{\pm}$, which could reach sizable branching fractions in certain parameter regions. With detailed collider analysis, we obtain the exclusion bounds as well as discovery reach at the 14 TeV LHC for the process $pp \to H^{\pm}tb \to AW^{\pm}tb/HW^{\pm}tb \to \tau\tau bbWW, bbbbWW$. We find that for a daughter particle mass of 50 GeV, the 95% C.L. exclusion reach in $\sigma \times$ BR varies from about 70 fb to 25 fb, for $m_{H^{\pm}}$ ranging from 150 GeV to 500 GeV with 300 fb^{-1} integrated luminosity in the $\tau\tau$ mode. We further interpret these bounds in the context of Type II Two Higgs Doublet Model. We find that large regions of parameter space in $\tan\beta$ versus $\sin(\beta-\alpha)$ can be covered when the daughter Higgs mass is relatively light, in particular, for small and large $\tan\beta$. The exclusion region in the $m_{H^{\pm}} - \tan\beta$ plane can be extended to $m_{H^{\pm}} = 600$ GeV, while discovery is possible for $m_{H^{\pm}} \lesssim 280$ GeV with 300 fb^{-1} integrated luminosity. The exotic decay mode $H^{\pm} \to AW^{\pm}/HW^{\pm}$ offers a complementary channel to the conventional mode $H^{\pm} \to \tau\nu$ for charged Higgs searches.

arXiv:1408.4119v1 [hep-ph] 18 Aug 2014

Contents

1 Introduction **2**

2 Scenarios with large $H^{\pm} \to AW^{\pm}/HW^{\pm}$ **3**

3 Current limits **6**

4 Collider analysis **7**
- 4.1 Signal process 7
- 4.2 $A \to \tau\tau$ mode 9
- 4.3 $A \to bb$ mode 13

5 Implication for the Type II 2HDM **15**
- 5.1 Cross section and branching fractions 15
- 5.2 Reach in parameter spaces 18

6 Conclusion **21**

1 Introduction

The discovery of the Standard Model (SM)-like Higgs at the LHC [1–4] marks the final and one of the most important discoveries within the SM of particle physics as regards its particle content. The ATLAS and CMS experiments have reported precise measurements of the mass of this particle, as well as the determination of its spin [2, 4, 5]. The present scenario raises interesting questions about the origin of Electroweak Symmetry Breaking (EWSB). It is conceivable that the scalar sector of the SM does indeed engineer all of EWSB, but at the same time we have compelling evidence from theoretical and experimental fronts that the SM needs to be supplanted with other dynamics for it to consistently explain issues like the naturalness problem, neutrino masses and the dark matter in the universe. Thus it is entirely possible that the scalar sector of the SM responsible for EWSB itself has a richer structure. Early attempts toward enlarging the scalar sector resulted in the Two Higgs Doublet Models (2HDM) [6–9]. Other examples also involving an enlarged scalar sector include the Minimal Supersymmetric Standard Model (MSSM) [10–12] and the Next to Minimal Supersymmetric Standard Model (NMSSM) [13, 14].

Models with extended Higgs sectors hold a lot of phenomenological interest. The discovery of extra Higgs bosons would serve as unambiguous evidence for new physics beyond the SM. A clear indication for a non-minimal Higgs sector as a source of EWSB would be the observation of charged Higgs bosons $H^\pm$ which are absent in the SM. The discovery of the charged Higgs, however, is quite challenging at colliders. If the mass of the charged Higgs $m_{H^\pm}$ is smaller than the top mass m_t, the dominant production mechanism of the charged Higgs is via top decay: $t \to bH^+$. Most studies performed at LEP, Tevatron and LHC focus on such light charged Higgs bosons which are assumed to either decay leptonically ($H^\pm \to \tau\nu$), or into jets ($H^\pm \to cs$). In the case of a heavy charged Higgs with $m_{H^\pm} > m_t$, the main production mode is the top quark associated production $H^\pm tb$. For the dominant decay $H^\pm \to tb$, it is difficult to identify the $ttbb$ signal given the huge irreducible SM backgrounds. The current heavy charged Higgs searches thus mostly focus on the subdominant decays $H^\pm \to \tau\nu$ or cs in order to take advantage of the cleaner signal and suppressed backgrounds.

Other possible decay channels like $H^\pm \to AW^\pm, HW^\pm$ open up once they are kinematically accessible, where H and A refer to the generic CP-even and CP-odd Higgs, respectively[1]. In the 2HDM, the couplings $H^\pm AW^\mp / H^\pm HW^\mp$ are controlled by the electroweak gauge coupling g. While the coupling to A is independent of the mixing angles, the coupling to H is maximized for non-SM-like CP-even Higgses. These exotic decays quickly dominate over $\tau\nu, cs$ once they are open, and could be even larger than the tb mode for a large range of $\tan\beta$. It was shown that in the 2HDM or NMSSM, both decays $H^\pm \to A_i W^\pm, H_i W^\pm$ could appear with large branching fractions[2] [15–17]. It is thus timely to study such charged Higgs decay channels and fully explore the experimental discovery potential for an enlarged

[1] Note that we use h^0 and H^0 to refer to the lighter or the heavier CP-even Higgs for models with two CP-even Higgs bosons. When there is no need to specify, we use H to refer to the CP-even Higgses.

[2] $H^\pm \to AW^\pm, HW^\pm$ is less likely to open in the MSSM due to kinematical constraints that force $m_{H^\pm} \sim m_A \sim m_H$ for the non SM-like Higgses.

Higgs sector.

In this paper, we focus on $H^\pm tb$ associated production of the charged Higgs with the subsequent exotic decay of $H^\pm \to AW^\pm/HW^\pm$. We consider leptonic decay of one of the $W^\pm$ either coming from $H^\pm$ or top decay, with the A/H in the final state decaying into a pair of fermions (bb or $\tau\tau$) and explore the exclusion bounds as well as the discovery reach at the LHC for various combinations of $(m_{H^\pm}, m_{H/A})$. ATLAS investigated this decay mode in an early study [18, 19] focusing on the $A/H \to bb$ mode only. So far no analysis has been done for the more promising $A/H \to \tau\tau$ mode.

A light charged Higgs could have a large impact on precision and flavor observables [20]. For example, in the 2HDM, the bounds on $b \to s\gamma$ restrict the charged Higgs to be heavier than 300 GeV. A detailed analysis of precision and flavor bounds in the 2HDM can be found in Refs. [21, 22]. Flavor constraints on the Higgs sector are, however, typically model-dependent, and could be alleviated when there are contributions from other new particles in the model. Our focus in this work is on collider searches for the charged Higgs and its implications for the Type II 2HDM. Therefore, we consider a wide range of charged Higgs mass.

The paper is organized as follows. In Sec. 2, we present a brief overview of models and parameter regions where $H^\pm \to AW^\pm/HW^\pm$ can be significant. In Sec. 3, we summarize the current experimental search limits on charged Higgses. Sec. 4 describes the collider analysis in detail. After describing the signal process and event generation in Sec. 4.1, we present the details of the analysis for the $A/H \to \tau\tau$ channel in Sec. 4.2. We show the model independent results of 95% C.L. exclusion as well as 5σ discovery limits for $\sigma(pp \to H^\pm tb \to A/HW^\pm tb \to \tau\tau bbWW)$ at the 14 TeV LHC with 100, 300 and 1000 fb^{-1} integrated luminosity. In Sec. 4.3 we present the analysis for the $H/A \to bb$ final state and derive the corresponding cross section limits. In Sec. 5, we study the implications of the collider search limits on the Type II 2HDM. We conclude in Sec. 6.

2 Scenarios with large $H^\pm \to AW^\pm/HW^\pm$

In the 2HDM, we introduce two SU(2)$_L$ doublets Φ_i, $i = 1, 2$:

$$\Phi_i = \begin{pmatrix} \phi_i^+ \\ (v_i + \phi_i^0 + iG_i)/\sqrt{2} \end{pmatrix}, \tag{2.1}$$

where v_1 and v_2 are the vacuum expectation values (vev) of the neutral components which satisfy the relation $\sqrt{v_1^2 + v_2^2} = 246$ GeV after EWSB. Assuming an additional discrete $\mathcal{Z}_2$ symmetry imposed on the Lagrangian, we are left with six free parameters, which can be chosen as the four Higgs masses (m_{h^0}, m_{H^0}, m_A, $m_{H^\pm}$), a mixing angle α between the two CP-even Higgses, and the ratio of the two vacuum expectation values, $\tan\beta = v_2/v_1$. In the case where a soft breaking of the $\mathcal{Z}_2$ symmetry is allowed, there is an additional parameter m_{12}^2.

The Higgs mass eigenstates containing a pair of CP-even Higgses (h^0, H^0), one CP-odd Higgs A and a pair of charged Higgses $H^\pm$ can be written as[3]:

$$\begin{pmatrix} H^0 \\ h^0 \end{pmatrix} = \begin{pmatrix} \cos\alpha & \sin\alpha \\ -\sin\alpha & \cos\alpha \end{pmatrix} \begin{pmatrix} \phi_1^0 \\ \phi_2^0 \end{pmatrix}, \quad \begin{aligned} A &= -G_1 \sin\beta + G_2 \cos\beta \\ H^\pm &= -\phi_1^\pm \sin\beta + \phi_2^\pm \cos\beta \end{aligned}. \tag{2.2}$$

The couplings that are of particular interest are of the type $H^\pm A W^\mp$ and $H^\pm H W^\mp$. They are determined by the gauge coupling structure, as well as the mixing angles [23]:

$$g_{H^\pm h^0 W^\mp} = \frac{g\cos(\beta-\alpha)}{2}(p_{h^0} - p_{H^\pm})^\mu, \tag{2.3}$$

$$g_{H^\pm H^0 W^\mp} = \frac{g\sin(\beta-\alpha)}{2}(p_{H^0} - p_{H^\pm})^\mu, \tag{2.4}$$

$$g_{H^\pm A W^\mp} = \frac{g}{2}(p_A - p_{H^\pm})^\mu, \tag{2.5}$$

with g being the $\mathrm{SU}(2)_L$ coupling, and p_μ being the incoming momentum for the corresponding particle.

An interesting feature here is that $H^\pm$ always couples to the non-SM-like CP-even Higgs more strongly. If we demand h^0 (H^0) to be SM-like, then $|\sin(\beta-\alpha)| \sim 1$ ($|\cos(\beta-\alpha)| \sim 1$), and the $H^\pm H^0 W^\mp$ ($H^\pm h^0 W^\mp$) coupling is unsuppressed. Therefore, in the h^0-126 case, $H^\pm$ is more likely to decay to $H^0 W^\pm$ than $h^0 W^\pm$ unless the former decay is kinematically suppressed. In the H^0-126 case, $H^\pm$ is more likely to decay to $h^0 W^\pm$ than $H^0 W^\pm$. The $H^\pm A W^\mp$ coupling, on the other hand, does not depend on any mixing angle and therefore this decay is not suppressed once it is kinematically allowed.

In the generic 2HDM, there are no mass relations between the charged scalars, the scalar and pseudoscalar states. Thus, the decays $H^\pm \to h^0 W^\pm$, $H^0 W^\pm$ and $H^\pm \to A W^\pm$ can all be kinematically accessible and dominate in different regions of parameter spaces. It was shown in Ref. [21] that in the Type II 2HDM with $\mathcal{Z}_2$ symmetry, imposing all experimental and theoretical constraints still left sizable regions in the parameter space that permit such exotic decays with unsuppressed decay branching fractions.

The dominant competing mode is $H^\pm \to tb$, which is controlled by the $H^\pm tb$ coupling

$$g_{H^\pm tb} = \frac{g}{2\sqrt{2}m_W}\left[(m_b \tan\beta + m_t \cot\beta) \pm (m_b \tan\beta - m_t \cot\beta)\gamma_5\right] \tag{2.6}$$

in the Type II 2HDM. At both small and large $\tan\beta$, $\Gamma(H^\pm \to tb)$ is increased given the enhanced top and bottom Yukawa coupling, respectively. The subdominant channel $H^\pm \to \tau\nu$ has similar enhancement at large $\tan\beta$ as well.

In the left panel of Fig. 1, we present contours of the branching fraction $\mathrm{BR}(H^\pm \to AW^\pm)$ in the $m_{H^\pm} - \tan\beta$ plane fixing $\sin(\beta-\alpha) = 1$, $m_A = 50$ GeV and decoupling H^0. It is seen that there is a "kink" at the tb threshold which brings down the steeply increasing values of $\mathrm{BR}(H^\pm \to AW^\pm)$. Even so, the $AW^\pm$ mode can be 90% or higher in the band $1.5 \lesssim \tan\beta \lesssim 30$ for $m_{H^\pm}$ between 175 and 600 GeV. For large or small values of $\tan\beta$, $\mathrm{BR}(H^\pm \to AW^\pm)$ is reduced due to competition from $H^\pm \to tb, \tau\nu$ modes.

[3]For more details about the 2HDM model, see Ref. [6].

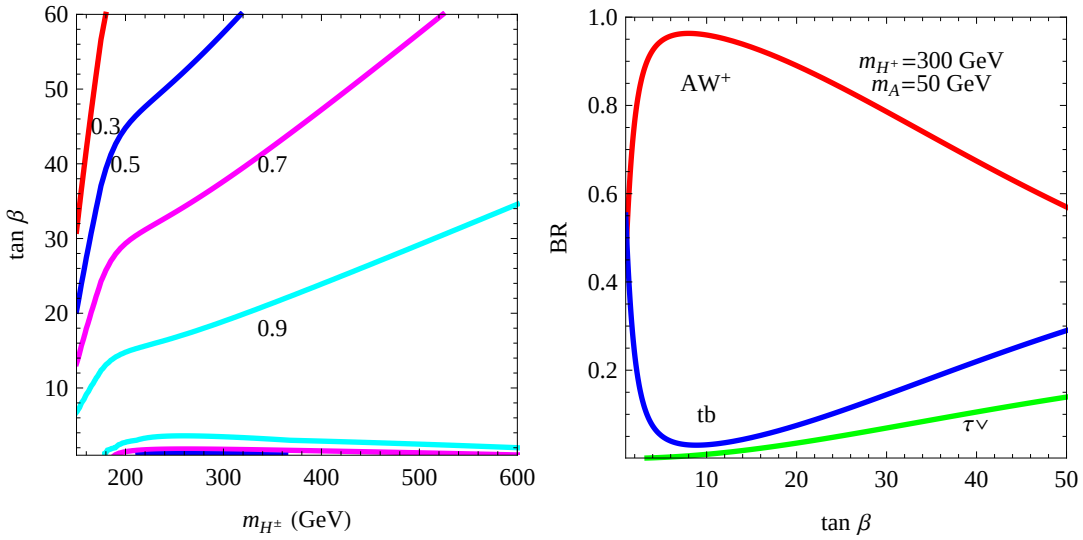

Figure 1. Left panel: Branching fraction BR($H^\pm \to AW^\pm$) in the $m_{H^\pm} - \tan\beta$ plane, for $m_A =$ 50 GeV and $\sin(\beta-\alpha)$ =1. Right panel: The branching fractions of $H^\pm$ as a function of $\tan\beta$ for various decay modes: $H^\pm \to AW^\pm$ (red), tb (blue), $\tau\nu$ (green) for $m_{H^\pm} = 300$ GeV, $m_A = 50$ GeV and $\sin(\beta-\alpha) = 1$.

The $H^\pm \to H^0W^\pm$ mode, when kinematically accessible, would show similar features with additional phase space suppression. $H^\pm \to h^0W^\pm$ mode is maximized at $\sin(\beta-\alpha) = 0$, which could be a potentially useful search channel for $H^\pm$ in the H^0- 126 case. The current searches for the charged Higgs focus on the $H^\pm \to \tau\nu$ channel, which is sensitive to the large $\tan\beta$ region. We expect the $H^\pm \to AW^\pm/HW^\pm$ channel to be complementary for small or intermediate $\tan\beta$.

In the right panel of Fig. 1, we show the branching fractions of $H^\pm$ as a function of $\tan\beta$ for various decay modes of $H^\pm \to AW^\pm$, $tb, \tau\nu$ for $m_{H^\pm} = 300$ GeV, $m_A = 50$ GeV and $\sin(\beta-\alpha) = 1$. For almost all values of $\tan\beta$, the decay to the $AW^\pm$ mode exceeds that of tb.

The Higgs sector in the MSSM is more restricted, given that the quartic Higgs couplings are fixed by the gauge couplings and the tree-level Higgs mass matrix only depends on m_A and $\tan\beta$. The decay $H^\pm \to h^0W^\pm$ is typically suppressed by the small coupling $\cos(\beta-\alpha) \sim 0$, and is only relevant for small $\tan\beta$. However, the authors of [24] showed that this channel can have a significant branching fraction in a small region of parameter space for small values of $\tan\beta$. In the usual decoupling region with large m_A, the light CP-even Higgs h^0 is SM-like while the other Higgses are almost degenerate: $m_{H^0} \sim m_A \sim m_{H^\pm}$. Thus, $H^\pm \to H^0W^\pm$ or $H^\pm \to AW^\pm$ is not kinematically allowed at tree-level. However, next-to-leading order (NLO) corrections can increase the mass difference between the charged and neutral Higgses for moderate values of $\tan\beta \approx 5$ to 10. In this case the $H^\pm \to A/H^0W^\pm$ channels can open up with significant branching fractions [25]. In the NMSSM, the Higgs sector of MSSM is enlarged to include an additional singlet. It was shown in Ref. [15] that in this model, there are regions of parameter space where the decay $H^\pm \to H_iW^\pm/A_iW^\pm$

can be significant.

3 Current limits

Searches for a light charged Higgs boson with mass $m_{H^\pm} < m_t$ have been performed both by ATLAS and CMS. The production mechanism considered is top pair production in which one top quark decays into a charged Higgs $t \to bH^\pm$ while the other top decays into bW. These studies mainly focus on the $H^\pm \to \tau\nu$ decay channel. The ATLAS [26, 27] study was performed with 19.5 fb^{-1} integrated luminosity at 8 TeV looking at the τ+jets final state and with 4.6 fb^{-1} integrated luminosity at 7 TeV using the τ+jets, τ+lepton and lepton+jets final states. Assuming a branching fraction BR($H^\pm \to \tau\nu$) = 100%, the null search results imply an upper bound for the top quark branching fraction BR($t \to bH^\pm$) = 0.24% to 2.1% for charged Higgs masses between 90 GeV and 160 GeV. This result can be translated into bounds on the MSSM parameter space. In the $m_h^{\rm max}$ scenario of the MSSM, this corresponds to an exclusion on $m_{H^\pm}$ of 100 GeV $< m_{H^\pm} <$ 140 GeV for all values of $\tan\beta$. Only small regions of parameter space at 90 GeV $< m_{H^\pm} <$ 100 GeV and 140 GeV $< m_{H^\pm} <$ 160 GeV around $\tan\beta = 10$ are still allowed. The limits from CMS [28] are relatively weak.

A search with the $H^\pm \to cs$ final state has been performed by ATLAS [29] using 4.7 fb^{-1} integrated luminosity at 7 TeV. Assuming BR($H^\pm \to cs$) = 100%, this implies an upper bound for the top quark branching fraction BR($t \to bH^\pm$) = 5% to 1% for charged Higgs masses between 90 GeV and 150 GeV.

The ATLAS collaboration [27] has also searched for a heavy charged Higgs boson with mass $m_{H^\pm} > m_t$ produced in association with a top quark. With 19.5 fb^{-1} integrated luminosity at 8 TeV and assuming a branching fraction BR($H^\pm \to \tau\nu$) = 100%, null search results implies an upper bound on the production cross section $\sigma(pp \to H^\pm tb)$ between 0.9 pb and 0.017 pb for charged Higgs masses in the range between 180 GeV and 600 GeV. When interpreting in the $m_h^{\rm max}$ scenario of the MSSM, $\tan\beta$ above 47 to 65 is excluded for $m_{H^\pm}$ between 230 to 310 GeV.

As demonstrated in Fig. 1, the conventional decay modes $\tau\nu$ and cs would be highly suppressed in regions of parameter space where the exotic decay modes $H^\pm \to AW^\pm/HW^\pm$ open. In Fig. 2, we recast the current 95% C.L. exclusion limits (solid red curve) [27] and future projection of 5σ discovery (solid blue curve) [30] with 100 fb^{-1} integrated luminosity at the 14 TeV LHC for the process $pp \to H^\pm tb \to (\tau\nu)(bbjj)$ in the context of the Type II 2HDM. The dashed curves show the reduced reach when $H^\pm \to AW^\pm$ opens up, shown here for the parameter choice $m_A = 50$ GeV, $\sin(\beta-\alpha) = 1$, and with the H^0 decoupled. The inclusion of the exotic decay modes thus substantially weakens the current and future limits.

There have been other theoretical studies on the charged Higgs detectability at the LHC. The authors of [31] analyzed the possibility of observing light charged Higgs decay $H^\pm \to \tau\nu$ via the single top production mode. The possibility of the $H^\pm \to \mu\nu$ decay with a light charged Higgs produced via top decay in top pair production has been investigated in [32]. Furthermore the decay of a heavy charged Higgs into tb has been studied, considering

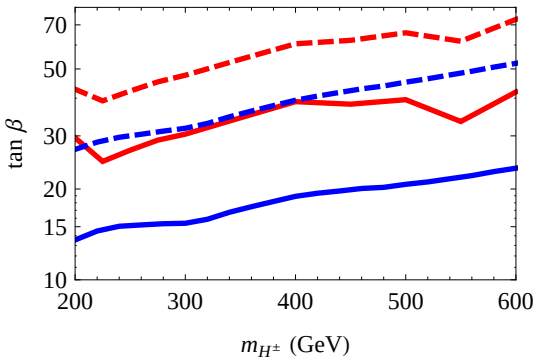

Figure 2. The recast of the current ATLAS 95% CL exclusion limits (solid red curves) [27] with 19.5 fb^{-1} integrated luminosity and the projected 5σ reach (solid blue curves) [30] with 100 fb^{-1} integrated luminosity at the 14 TeV LHC for the process $pp \to H^\pm tb \to (\tau\nu)(bbjj)$ in the context of the Type II 2HDM. Also shown in dashed curves are the reduced limits with the opening of $H^\pm \to AW^\pm$, with $m_A = 50$ GeV, $\sin(\beta - \alpha) = 1$ and H^0 decoupled.

charged Higgs production via $qq' \to H^\pm$ [33], $H^\pm tb$ associate production [34] and $W^\mp H^\pm$ associate production [35].

Furthermore, the authors of [36] studied electroweak charged Higgs boson pair production with the charged Higgses decaying into a W boson and a very light [$m_\phi = \mathcal{O}(eV)$] neutral scalar which decays invisibly. A search strategy for $H^\pm \to h^0 W^\pm$ for a SM-like h^0 using the $H^\pm W^\mp$ production mode has been suggested by the authors of [37] and analysed in the context of CP-violating Type-II 2HDM. This study considers both electroweak production and the production via the decay of heavy scalars, if it is kinematically allowed. Charged Higgs production via the decay of a heavy scalar $pp \to H \to WH^\pm$ with $H^\pm \to AW^\pm$ was investigated in [38].

The $H^\pm tb$ associated production with $H^\pm \to HW^\pm \to bbW^\pm$ has been analyzed in early studies [18, 19]. While Ref. [18] concluded that the $H^\pm \to h^0 W^\pm / H^0 W^\pm$ is not promising in MSSM searches, the authors of [19] found that this channel is indeed promising in NMSSM. However, neither paper considers the possibility of analyzing this channel with the $\tau\tau$ mode. In particular, the $\tau\tau$ mode allows two same sign lepton signature with the accompanying leptonic decay of W [39], which leads to a better reach than the existing studies of the $H/A \to bb$ channel. Therefore, in our study, we analyze the discovery and exclusion prospects in both $H^\pm \to AW^\pm / HW^\pm \to bbW^\pm$ and $H^\pm \to AW^\pm / HW^\pm \to \tau\tau W^\pm$ channels.

4 Collider analysis

4.1 Signal process

In our analysis we study the associated production $pp \to H^\pm tb$ in which the charged Higgs boson decays into a neutral Higgs (A or H) and a W. The leading order Feynman diagrams contributing to this production are shown in Fig. 3 [40]. For large charged Higgs masses, diagrams (a) and (b) dominate while for smaller charged Higgs masses, top pair production

in panel (c) with the decay of one (possibly offshell) top into a charged Higgs dominates. The exclusion and discovery reach in $\sigma \times$ BR obtained in this section will cover the entire kinematically possible mass range. When interpreting the results in the Type II 2HDM in Sec. 5, we focus on the high mass region: $m_{H^\pm} > m_t$. For the low mass range where the $t\bar{t}$ production dominates, the bounds are usually translated into limits on the branching fraction BR$(t \to H^\pm b)$ [41].

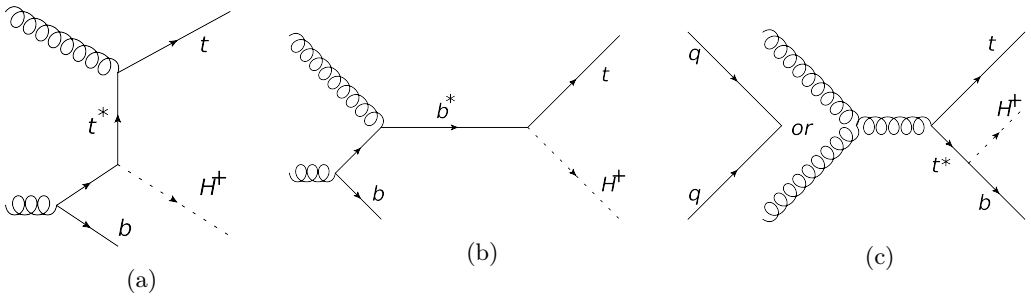

Figure 3. t-channel (a), s-channel (b) and $t\bar{t}$-like (c) diagrams contributing to heavy quark associated charged Higgs production [40].

In principle the neutral Higgs boson can either be CP-even (denoted by H) or CP-odd (denoted by A). In the analysis that follows, we use the decay $H^\pm \to AW^\pm$ as an illustration. Since we do not make use of angular correlations, the bounds obtained for $H^\pm \to AW^\pm$ apply to $H^\pm \to HW^\pm$ as well.

The neutral Higgs boson itself will further decay. We only look at the fermionic decays $A \to bb, \tau\tau$. While the bb case has the advantage of a large branching fraction BR$(A \to bb)$, the $\tau\tau$ case has less SM backgrounds and therefore leads to a cleaner signal. We study both leptonic and hadronic τ decays and consider the three cases: $\tau_{had}\tau_{had}$, $\tau_{lep}\tau_{had}$ and $\tau_{lep}\tau_{lep}$. The $\tau_{lep}\tau_{had}$ case is particularly promising since we can utilize the same sign dilepton signal with the leptons from W decay and from τ decay. Exotic decays of A/H into pairs of vector bosons or other Higgs bosons will most likely be suppressed or have a very complex final state. Since the top quark decays to bW, the final state contains two W bosons. To reduce the backgrounds, in our analysis we assume one of these two W bosons decays leptonically, with the other W decaying hadronically.

We use Madgraph 5/MadEvent v1.5.11 [42] to generate our signal and background events. These events are passed to Pythia v2.1.21 [43] to simulate initial and final state radiation, showering and hadronization. The events are further passed through Delphes 3.07 [44] with the Snowmass combined LHC detector card [45] to simulate detector effects. The discovery reach and exclusion bounds have been determined using the program theta-auto [46].

In this section, we will present model *independent* limits on the $\sigma \times$ BR for both 95% C.L. exclusion and 5σ discovery for both possible final states $\tau\tau bbWW$ and $bbbbWW$. For the signal process, we generated event samples at 14 TeV LHC for $pp \to H^\pm tb \to AW^\pm tb$ with the daughter particle mass fixed at $m_A = 50, 126, 200$ GeV to represent the cases with a light, SM-like, and a heavy Higgs respectively. For each case, we vary the parent particle mass $m_{H^\pm}$ in the range $150 - 600$ GeV.

4.2 $A \to \tau\tau$ mode

We start our analysis by looking at the channel $pp \to H^{\pm}tb \to AW^{\pm}tb \to \tau\tau bbWW$. We only require to identify one b jet from top decay. We do not require to find the b jet produced in association with the charged Higgs since it is likely to be soft. As mentioned above, we will distinguish three cases depending on how the taus decay:

- **Case A:** Both taus decay hadronically.
- **Case B:** One tau decays hadronically, and the other tau decays leptonically.
- **Case C:** Both taus decay leptonically.

For the two W bosons, we require one decay leptonically and the other decay hadronically. The dominant SM background for this final state is semi- and fully leptonic (where leptonic includes decaying into τ) $t\bar{t}$ pair production, which we generate with up to one additional jet. We also take into account $tt\tau\tau$ production, where the taus come from the decay of a boson $Z/H/\gamma^*$. Furthermore we include $W\tau\tau$ production with up to two additional jets (including b jets) and $WW\tau\tau$ production with up to one additional jet (including b jet), where the taus are produced in the decay of a boson $Z/H/\gamma^*$. We ignored the subdominant backgrounds from single vector boson production, WW, ZZ, single top production, as well as multijet QCD Background. Those backgrounds are either small or can be sufficiently suppressed by the cuts imposed.

We apply the following cuts to extract the signal from the backgrounds:

1. **Identification cuts:**
   Case A: One lepton $\ell = e$ or μ , one or two b jets, two τ tagged jets and at least two untagged jets:
   $$n_\ell = 1,\ n_b = 1, 2,\ n_\tau = 2,\ n_j \geq 2. \tag{4.1}$$
   We require that the τ tagged jets have opposite charge.

   Case B: Two leptons, one or two b jets, one τ tagged jet and at least two untagged jets:
   $$n_\ell = 2,\ n_b = 1, 2,\ n_\tau = 1,\ n_j \geq 2. \tag{4.2}$$
   We require that both leptons have the same sign, which is opposite to the sign of the τ tagged jet.

   Case C: Three leptons, one or two b jets, no τ tagged jet and at least two untagged jets:
   $$n_\ell = 3,\ n_b = 1, 2,\ n_\tau = 0,\ n_j \geq 2. \tag{4.3}$$
   We adopt the following selection cuts for the identification of leptons, b jets and jets.
   $$|\eta_{\ell,b,\tau}| < 2.5,\ |\eta_j| < 5,\ p_{T;\ell_1,j,b} > 20 \text{ GeV and } p_{T;\ell_2} > 10 \text{ GeV}, \tag{4.4}$$
   where $\ell_{1,2}$ refer to the hardest and the sub-leading lepton. For jet reconstruction, the anti-k_T jet algorithm with $R = 0.5$ is used.

2. **Two W candidates:** Our analysis assumes that one W decays leptonically and the other decays hadronically. We look for the combination of two untagged jets that gives an invariant mass closest to the W mass and reconstruct the jets to form the hadronic W_{had}. The momentum of the neutrino coming from the leptonic W decay is determined using the missing transverse momentum and imposing the mass conditions [47]. Using the momenta of the reconstructed neutrino and the lepton, the momentum of the leptonic W_{lep} can be deduced. In cases B and C which contain more than one lepton, the hardest lepton is used for W reconstruction. In these cases the neutrino reconstruction will be relatively poor since there is additional missing energy from the τ decay.

3. **Top candidate:** We look for the combination of the b tagged jet and a reconstructed (either leptonic or hadronic) W that gives an invariant mass closest to the top mass and combine them to form the top candidate t.

4. **Neutral Higgs candidate (H):** The τ jets (case A), the τ jet and the softer lepton (case B) or the two softer leptons (case C) are combined to form the neutral Higgs candidate. In cases B and C the Higgs reconstruction will be relatively poor for reasons mentioned above which in turn forces us to employ more relaxed mass cuts (see below).

5. **Charged Higgs candidate ($H^{\pm}$):** The Higgs candidate and the W candidate not used for the top reconstruction are combined to form the charged Higgs candidate $H^{\pm}$.

6. **$m_{\tau\tau}$ versus $m_{\tau\tau W}$:** We require the ditau mass $m_{\tau\tau}$ to be close to the daughter Higgs mass m_A and the mass of the two taus and the W ($m_{\tau\tau W}$) to be close to the parent Higgs mass $m_{H^{\pm}}$. The two masses are correlated, i.e., if we underestimate $m_{\tau\tau}$ we also underestimate $m_{\tau\tau W}$. To take this into account we apply a two-dimensional cut:

$$\begin{aligned} (1-\Delta-w_{\tau\tau})\cdot m_A < \; & m_{\tau\tau} < (1-\Delta+w_{\tau\tau})\cdot m_A, \\ \frac{m_A}{E_A}(m_{\tau\tau W}-m_{H^{\pm}}-w_{\tau\tau W}) < m_{\tau\tau}-m_A < & \frac{m_A}{E_A}(m_{\tau\tau W}-m_{H^{\pm}}+w_{\tau\tau W}). \end{aligned} \tag{4.5}$$

Here $w_{\tau\tau} = 0.225$ (case A) or 0.25 (cases B and C) is the width of the ditau mass window. Note that the slightly shifted reconstructed Higgs mass $m_{\tau\tau}$ around $(1-\Delta)m_A$ instead of m_A is due to the reconstruction of the τ using a jet with a small size of $R = 0.5$ or a lepton. We use $\Delta = 0.3$ (case A), 0.4 (case B) and 0.66 (case C). The second condition describes two lines going through the points $(m_{H^{\pm}} \pm w_{\tau\tau W}, m_A)$ with slope $\frac{m_A}{E_A}$ where E_A is the energy of the neutral Higgs in the rest frame of the charged Higgs[4]. We choose a width for the $m_{\tau\tau W}$ peak of $w_{\tau\tau W} = 0.2 m_{H^{\pm}}$, based on the theoretical decay width estimation of $w_{H^{\pm}} \sim 0.1 m_{H^{\pm}}$ as well as detector resolutions.

[4]We choose $E_A = \frac{m_{H^{\pm}}^2 + m_A^2 - m_W^2}{2m_A}$, which is the energy of A in the rest frame of the charged Higgs. The slope in Eq. (4.5) can be motivated by relativistic kinematics and works well even when the charged Higgs is not produced at rest.

The effectiveness of this cut is shown in Fig. 4 for $m_{H^\pm} = 240$ GeV and $m_A = 50$ GeV in case A, with two horizontal lines indicating the $m_{\tau\tau}$ range and two slanted lines indicating the $m_{\tau\tau W}$ range as given in Eq. (4.5).

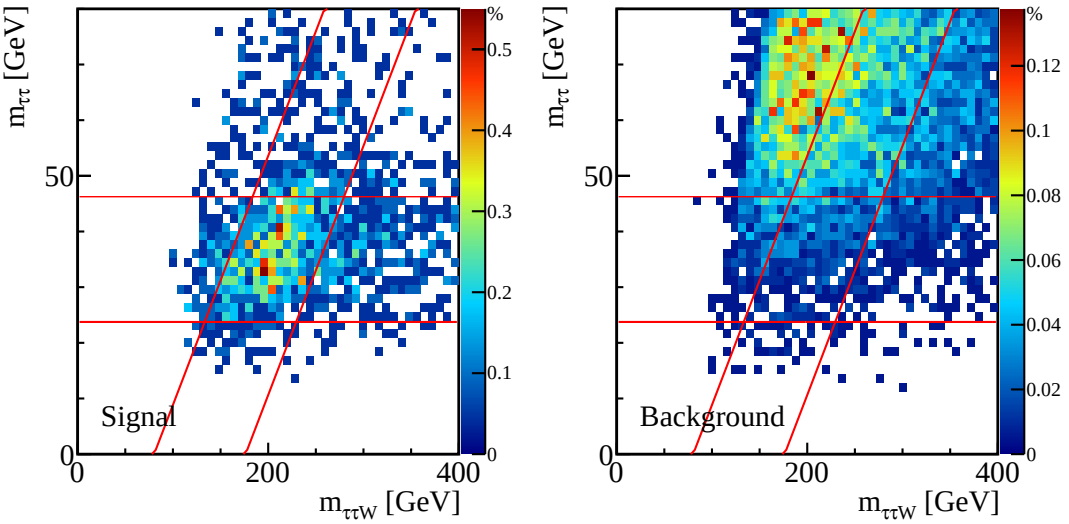

Figure 4. Normalized distribution (in percent as given by the color code in the panel along the y-axis) of $m_{\tau\tau}$ versus $m_{\tau\tau W}$ for the signal (left) and the backgrounds (right) assuming $m_{H^\pm} = 240$ GeV and $m_A = 50$ GeV for case A. Two horizontal lines indicate the $m_{\tau\tau}$ range and two slanted lines indicate the $m_{\tau\tau W}$ range, as given in Eq. (4.5).

No mass cuts are applied for the reconstructed W and t candidates since both signal and the dominant backgrounds contain a top quark and an additional W boson. In Table 1, we show the signal and background cross sections with cuts for a signal benchmark point of $M_{H^\pm} = 240$ GeV and $m_A = 50$ GeV at the 14 TeV LHC. The first row shows the total cross section before cuts calculated using MadGraph. The following rows show the cross sections after applying the identification cuts and mass cuts for all three cases as discussed above. We have chosen a nominal value for $\sigma \times BR(pp \to H^\pm tb \to \tau\tau bbWW)$ of 100 fb[5] to illustrate the cut efficiencies for the signal process. The last column shows the $S/\sqrt{B}$ value for an integrated luminosity of 300 fb^{-1}.

We can see that the dominant background contributions are $t\bar{t}$ (case A) and $t\bar{t}\tau\tau$ (cases B and C) while the vector boson backgrounds do not contribute much. It turns out that case B, in which one τ decays leptonically and the other τ decays hadronically, gives the best reach. This is because the same sign lepton signature can reduce the $t\bar{t}$ background sufficiently. This analysis is sensitive to the tagging and misidentification rate of the τ tagger. Most of the top pair background, especially in case A, includes mistagged τ jets. We assume a tagging rate of $\epsilon_{tag} = 60\%$ and a mistagging rate of $\epsilon_{miss} = 0.4\%$ as suggested

[5]For the Type II 2HDM the cross section for $m_{H^\pm} = 240$ GeV is typically in the range of $\sigma(pp \to H^\pm tb) = 0.1-1.5$ pb (see Fig. 7.). Assuming a branching fraction BR$(H^\pm \to AW^\pm) = 100\%$ and BR$(A \to \tau\tau) = 10\%$ leads to the stated $\sigma\times$ BR of around 100 fb.

Cut	Signal [fb]	$t\bar{t}$ [fb]	$t\bar{t}\tau\tau$ [fb]	$W(W)\tau\tau$ [fb]	S/B	$S/\sqrt{B}$
σ	100	$6.3 \cdot 10^5$	247	2000	-	-
A: Identification [Eq.(4.1)]	0.45	23.4	0.58	0.078	0.02	1.62
$m_{\tau\tau}$ vs $m_{\tau\tau W}$ [Eq.(4.5)]	0.14	0.69	0.014	0.003	0.19	2.84
B: Identification [Eq.(4.2)]	0.39	0.35	0.697	0.072	0.35	6.49
$m_{\tau\tau}$ vs $m_{\tau\tau W}$ [Eq.(4.5)]	0.13	0.043	0.047	0.0062	1.35	7.31
C: Identification [Eq.(4.3)]	0.44	2.35	5.11	0.058	0.06	2.81
$m_{\tau\tau}$ vs $m_{\tau\tau W}$ [Eq.(4.5)]	0.12	0.30	0.31	0.0077	0.19	2.54

Table 1. Signal and background cross sections with cuts for the signal benchmark point $m_{H^\pm} = 240$ GeV and $m_A = 50$ GeV at the 14 TeV LHC. We have chosen a nominal value for $\sigma \times \text{BR}(pp \to H^\pm tb \to \tau\tau bbWW)$ of 100 fb to illustrate the cut efficiencies for the signal process. The last column of $S/\sqrt{B}$ is shown for an integrated luminosity of $\mathcal{L} = 300$ fb^{-1}.

in [45]. A better rejection of non-τ initiated jets would increase the significance of this channel.

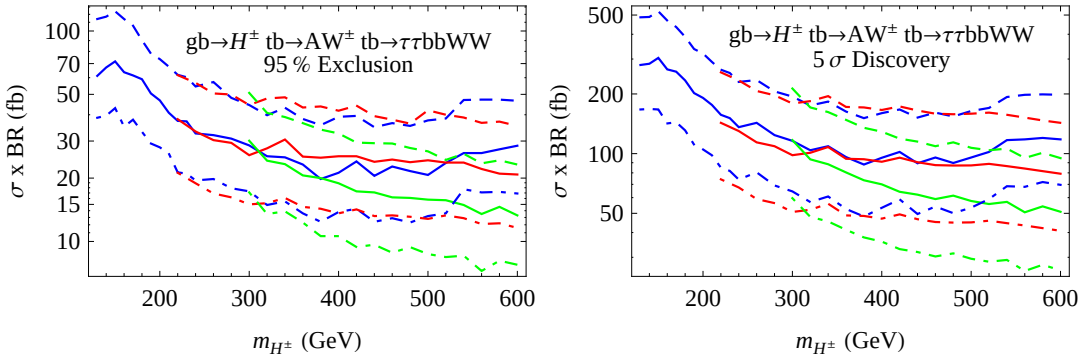

Figure 5. The 95% C.L. exclusion (left) and 5σ discovery (right) limits for $\sigma \times \text{BR}(pp \to H^\pm tb \to \tau\tau bbWW)$ for $m_A = 50$ GeV (blue), 126 GeV (red), and 200 GeV (green) at the 14 TeV LHC. We have combined all three cases of tau decays. The dashed, solid and dot-dashed lines correspond to an integrated luminosity of 100, 300 and 1000 fb^{-1}, respectively. Here, we have assumed a 10% systematic error on the backgrounds. These results are equally applicable to the $H^\pm \to HW^\pm$ process for the same parent and daughter Higgs masses.

In Fig. 5, we display the results at the 14 TeV LHC for 95% C.L. exclusion (left panel) and 5σ discovery (right panel) limits for $\sigma \times \text{BR}(pp \to H^\pm tb \to \tau\tau bbWW)$, which applies for $H^\pm \to HW^\pm$ as well with m_A replaced by m_H. We have combined all three cases of tau decays. The blue, red, and green curves correspond to the daughter particle being 50 GeV, 126 GeV, and 200 GeV, respectively. For each mass, we have displayed the results for three luminosities: 100 fb^{-1} (dashed), 300 fb^{-1} (solid), and 1000 fb^{-1} (dot-dashed), with 10% systematic error included [46]. Due to the small number of events, the statistical error dominates in this channel and therefore higher luminosities lead to a better reach. Better sensitivity is achieved for larger $m_{H^\pm}$ since the mass cuts on $m_{\tau\tau}$ and $m_{\tau\tau W}$ have a more pronounced effect on the SM backgrounds for larger masses.

The $m_{\tau\tau}$ distribution for the dominating tt backgrounds peaks around higher masses $m_{\tau\tau} \approx 70$ - 200 GeV and therefore the background rejection efficiency for $m_{\tau\tau} \approx 50$ GeV is

high compared to the cases with larger daughter particle masses. On the other hand a small daughter Higgs mass causes the taus to be either soft (low $m_{H^\pm}$) or collimated (high $m_{H^\pm}$) and decreases the identification efficiency compared to higher daughter particles masses. Taking into account these two effects, the limits do not change significantly for different daughter particle masses.

The limit, however, gets worse for the $m_A = 50$ GeV case when $m_{H^\pm} \gtrsim 400$ GeV (blue curves). This is due to the decrease of the signal cut efficiency for a highly boosted daughter particle with two collimated τ jets. For the interesting case where the daughter particle is 50 GeV, it is seen that the exclusion limits for a 300 fb^{-1} collider fall from about 70 fb for $m_{H^\pm}$ of 150 GeV, to less than 25 fb for a 500 GeV charged Higgs. The 5σ discovery limits are about a factor of 3−4 higher.

We reiterate here these exclusion and discovery limits are completely model independent. Whether or not discovery/exclusion is actually feasible in this channel should be answered within the context of a particular model, in which the theoretically predicted cross sections and branching fractions can be compared with the exclusion or discovery limits. We will do this in Sec. 5 using the Type II 2HDM as a specific example.

4.3 $A \to bb$ mode

We now turn to the channel $pp \to H^\pm tb \to bbbbWW$, with one W decaying leptonically and the other decaying hadronically. The dominant SM backgrounds for this final state are semi- and fully leptonic top pair production, which we generate with up to one additional jet. We also take into account $ttbb$ production where the two bottom jets either come from the decay of a boson $Z/H/\gamma^*$ or are produced through gluon splitting. We have ignored the subdominant backgrounds including V+jets, VV+jets or VVV+jets, single top production, as well as multijet QCD Background. These backgrounds either have small production cross sections, or can be sufficiently suppressed by the cuts imposed.

Much of the analysis for this case is similar to the $\tau\tau$ case described above. We apply the following cuts to identify the signal from the backgrounds:

1. **One lepton, three or 4 b jets, at least two untagged jets:**

$$\begin{gathered} n_\ell = 1,\ n_b = 3, 4,\ n_j \geq 2 \text{ with} \\ |\eta_{\ell,b}| < 2.5,\ |\eta_j| < 5,\ p_{T,\ell,j,b} > 20 \text{ GeV}. \end{gathered} \tag{4.6}$$

2. **Two W candidates and one top candidate:** Similar to that in Sec. 4.2. For top reconstruction, we look for the combination of a b tagged jet and a reconstructed W that gives an invariant mass closest to the top mass.

3. **Neutral Higgs candidate (A):** The remaining b jets are combined to form the Higgs candidate A with mass m_{bb}.

4. **Charged Higgs candidate ($H^\pm$):** The Higgs candidate and the W candidate not used for the top reconstruction are combined to form the charged Higgs candidate $H^\pm$ with mass m_{bbW}.

5. m_{bb} **versus** m_{bbW}**:** There is no Higgs mass shift Δ as in the $\tau\tau$ case since there is no missing energy carried away by neutrinos from tau decay anymore. Our 2-D cuts are thus modified as follows:

$$\begin{aligned} (1-w_{bb})\cdot m_A < \; m_{bb} < (1+w_{bb})\cdot m_A, \\ \frac{m_A}{E_A}(m_{bbW}-m_{H^\pm}-w_{bbW}) < m_{bb}-m_A < \frac{m_A}{E_A}(m_{bbW}-m_{H^\pm}+w_{bbW}). \end{aligned} \tag{4.7}$$

The mass window chosen is slightly tighter due to a better mass reconstruction in the bb case: $w_{bb} = 0.2$ and $w_{bbW} = 0.175 m_{H^\pm}$.

In Table 2, we present the cross sections after the individual cuts are imposed sequentially. We take a nominal signal cross section of 1000 fb to illustrate the efficiency of the chosen cuts. Since the expected number of events is large, the systematic uncertainty will dominate and a large ratio S/B is desired. Although $S/\sqrt{B}$ does not improve using the mass cut , S/B improves and therefore the systematic uncertainty, which dominates the overall uncertainty, decreases. The dominant background comes from top pair production.

Cut	Signal [fb]	$t\bar{t}$ [fb]	$t\bar{t}bb$ [fb]	S/B	$S/\sqrt{B}$
σ	1000	$6.5\cdot 10^5$	11310	-	-
Identification [Eq.(4.6)]	10.8	903	143	0.010	5.7
m_{bb} vs m_{bbW} [Eq.(4.7)]	0.53	15.1	1.8	0.031	2.8

Table 2. Signal and background cross sections with cuts for the signal benchmark point $m_{H^\pm} = 240$ GeV and $m_A = 50$ GeV at the 14 TeV LHC. We have chosen a nominal value for $\sigma \times BR(pp \to H^\pm tb \to bbbbWW)$ of 1000 fb to illustrate the cut efficiencies for the signal process. The last column of $S/\sqrt{B}$ is shown for an integrated luminosity of $\mathcal{L} = 300$ fb^{-1}.

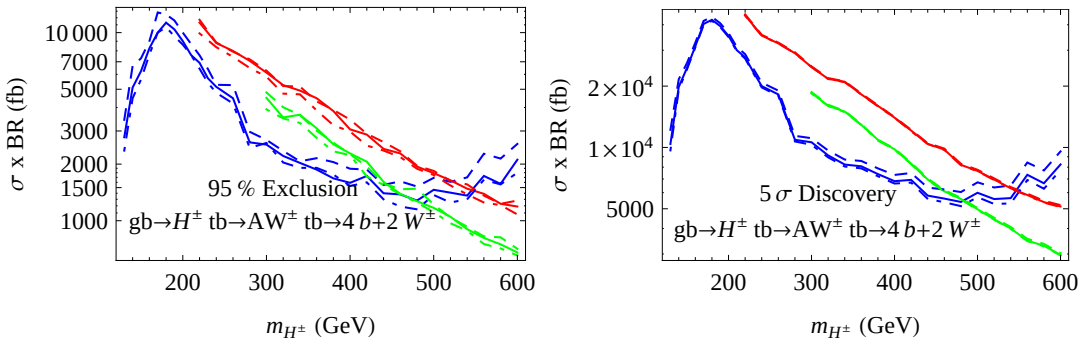

Figure 6. The 95% C.L. exclusion (left) and 5σ discovery (right) limits for $\sigma \times \mathrm{BR}(pp \to H^\pm tb \to bbbbWW)$ for $m_A = 50$ GeV (blue), 126 GeV (red), and 200 GeV (green) at the 14 TeV LHC. The dashed, solid and dot-dashed lines correspond to an integrated luminosity of 100, 300 and 1000 fb^{-1} respectively. Here, we have assumed a 10% systematic error on the backgrounds.

In Fig. 6, we show the 95% C.L. exclusion and 5σ discovery reach in $\sigma \times \mathrm{BR}(pp \to H^\pm tb \to bbbbWW)$ for the 14 TeV LHC. The general feature of these plots follows that of Fig. 5, particularly with highly boosted daughter particles making b identification more

challenging, as shown by the flattening and even slightly increasing of the blue curves for 50 GeV daughter particle mass when $m_{H^\pm} \gtrsim 450$ GeV. Unlike the $\tau\tau$ case, different luminosities do not change the limits significantly as the errors on the backgrounds are dominated by systematic uncertainties. Thus, in our analysis, we have chosen a uniform 10% systematic error on the backgrounds. With the possible reduction of systematic errors in the future, the cross section limits can be improved. For example, a 5% systematic error would lead to the cross section limits improved by about a factor of 2. The exclusion limits are lowest for small $m_A = 50$ GeV since the dominating $t\bar{t}$ background peaks around $m_{bb} \approx 70-200$ GeV and therefore the background rejection efficiency for $m_{bb} \approx 50$ GeV is high. The improvement of the sensitivity for the $m_A = 50$ GeV case when $m_{H^\pm} < 200$ GeV is due to the suppression of the $t\bar{t}$ background with the m_{bbW} cut.

Compared to the $\tau\tau$ case, the $\sigma \times$ BR reach in the bb case is worse due to significantly higher SM backgrounds. For the 50 GeV daughter particle case with 300 fb^{-1}, the exclusion limit varies from about 10 pb for a parent mass of 200 GeV to about 1.5 pb for 500 GeV. Thus, given the typical ratio of BR $(A/H \to bb) : \mathrm{Br}(A/H \to \tau\tau) \sim 3m_b^2/m_\tau^2$, we conclude that the reach in the bb case is much worse than that in the $\tau\tau$ case for all masses.

5 Implication for the Type II 2HDM

The discussion thus far has been completely model independent, and the discovery and exclusion limits displayed in Figs. 5 and 6 apply to any model in which $H^\pm \to AW^\pm/HW^\pm$ occurs. In this section, we will analyze the feasibility of this channel at the 14 TeV LHC in the context of the Type II 2HDM.

5.1 Cross section and branching fractions

In the Type II 2HDM, one Higgs doublet Φ_1 provides masses for the down-type quarks and charged leptons, while the other Higgs doublet Φ_2 provides masses for the up-type quarks. The couplings of the CP-even Higgses h^0, H^0 and the CP-odd Higgs A to the SM particles can be found in Ref. [6].

The discovery of the 126 GeV SM-like Higgs imposes restrictions on the couplings and masses of the various Higgses in the 2HDM, and several studies in the literature mapped out the available parameter space after all the theoretical and experimental constraints are imposed [16, 17, 21, 48, 49]. Note that the 2HDM offers two possibilities: either the h^0 or the H^0 could be interpreted as the observed 126 GeV resonance, and accordingly, the available parameter spaces differ. In the h^0-126 case with $m_{12}^2 = 0$, we are restricted to narrow regions with $\sin(\beta - \alpha) \sim \pm 1$ with $\tan\beta$ up to 4 or an extended region in $0.55 < \sin(\beta - \alpha) < 0.9$ with $1.5 < \tan\beta < 4$. The masses $m_{H^0}, m_{H^\pm}$, and m_A are, however, relatively unconstrained. In the H^0-126 case with $m_{12}^2 = 0$, we are restricted to a narrow region of $\sin(\beta-\alpha) \sim 0$ with $\tan\beta$ up to about 8, or an extended region of $\sin(\beta-\alpha)$ between -0.8 to -0.05, with $\tan\beta$ extending to 30 or higher [21]. m_A and $m_{H^\pm}$ are nearly degenerate due to $\Delta\rho$ constraints. Imposing the flavor constraints further narrows down the preferred parameter space. In what follows, we will specify the Higgs masses for each

benchmark point considered, but will display our results for all values of $\sin(\beta-\alpha)$ and $\tan\beta$.

Fig. 7 shows contours of NLO $\sigma(gg \to H^\pm tb)$ in the $m_{H^\pm} - \tan\beta$ plane at the 14 TeV LHC, with values taken from the LHC Higgs Working Group [50][6]. The production is controlled by the $H^\pm tb$ vertex, which is given in Eq. (2.6). This coupling is enhanced for both small and large $\tan\beta$, due to the enhancement of the top and bottom Yukawa coupling, respectively. Correspondingly, the cross section can reach up to 1.5 pb for $m_{H^\pm} \leq 300$ GeV for either $\tan\beta > 40$, or $\tan\beta < 2$. However, we note that the cross section decreases rapidly with increasing mass, falling below 50 fb in most regions of $m_{H^\pm} > 400$ GeV. This makes the charged Higgs search challenging in the high mass regions unless we get a particularly clean signal with minimal backgrounds.

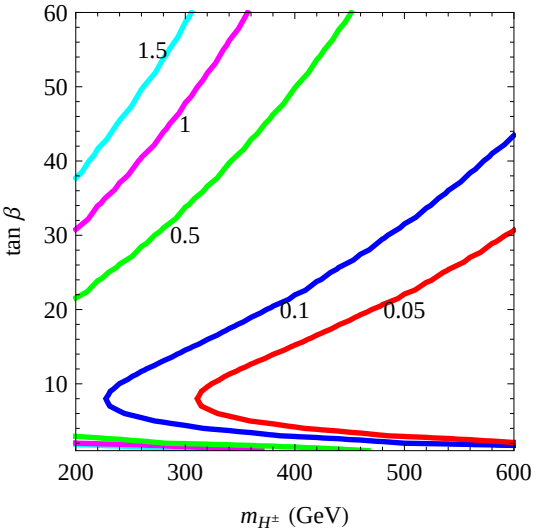

Figure 7. Contours of NLO $\sigma(pp \to H^\pm tb)$ (in pb) in the $m_{H^\pm} - \tan\beta$ plane at the 14 TeV LHC for the Type II 2HDM.

The results of Sec. 4, in principle, could be interpreted within the context of three processes: $H^\pm \to AW^\pm$, $H^\pm \to h^0 W^\pm$, and $H^\pm \to H^0 W^\pm$. The decay width of the first of these is independent of $\sin(\beta-\alpha)$, while decay to $h^0W^\pm$ or $H^0W^\pm$ is proportional to $\cos(\beta-\alpha)$ or $\sin(\beta-\alpha)$. Therefore, the decay to non-SM-like Higgs is preferable. In this section, we will consider two cases for illustration: i) $H^\pm \to AW^\pm$ for the h^0-126 case with H^0 decoupled and ii) $H^\pm \to h^0W^\pm$ for the h^0-126 and H^0-126 cases with A decoupled. We do not consider the decay $H^\pm \to H^0W^\pm$ as its reach is similar to the $H^\pm \to AW^\pm$ channel in the h^0-126 case while being suppressed in the H^0-126 case. We do not consider the decay $H^\pm \to AW^\pm$ in the H^0-126 case since the reach is always worse that that in the h^0-126 case due to competition from the $H^\pm \to h^0W^\pm$ mode.

We list the specific benchmark points considered in Table 3. BP1 and BP2 are chosen to illustrate the reach for the $H^\pm \to AW^\pm$ decay. A smaller $m_{H^\pm}$ is chosen for BP1

[6]The NLO cross sections are available only for $m_{H^\pm} \geq$200 GeV. Thus, for $m_{H^\pm}$ less than this value, we simply using the leading order numbers calculated using FeynHiggs [51].

to illustrate the effect of a larger production cross section. BP3 and BP4 are chosen to illustrate the reach for the $H^\pm \to h^0 W^\pm$ decay, with unsuppressed decay in BP3 (H^0-126 case) and suppressed decay in BP4 (h^0-126 case) when preferred value of $\sin(\beta-\alpha)$ is considered. Note that BP1 and BP4 admit only one exotic decay ($AW^\pm$ for the former and $h^0W^\pm$ for the latter), thus representing the simplest scenario where the reach is maximized in these two modes for the chosen $m_{H^\pm}$ value.

$\{m_{H^\pm}, m_A, m_{h^0}, m_{H^0}\}$ GeV	$H^\pm \to AW^\pm$	$H^\pm \to h^0W^\pm$	Favored Region
BP1: $\{200, 50, 126, 700\}$	✓	✗	$\sin(\beta-\alpha) \approx \pm 1$
BP2: $\{300, 126, 126, 700\}$	✓	✓	$\sin(\beta-\alpha) \approx \pm 1$
BP3: $\{300, 700, 50, 126\}$	✗	✓	$\sin(\beta-\alpha) \approx 0$
BP4: $\{300, 700, 126, 700\}$	✗	✓	$\sin(\beta-\alpha) \approx \pm 1$

Table 3. Benchmark points shown for illustrating the discovery and exclusion limits for the processes $pp \to H^\pm tb \to AW^\pm/HW^\pm tb \to \tau\tau bbWW$ in the context of Type II 2HDM. The checkmarks indicate kinematically allowed channels. Also shown are the typical favored region of $\sin(\beta-\alpha)$ for each case (see Ref. [21]).

In Fig. 8, we display the branching fraction of the $H^\pm \to AW^\pm$ and $h^0W^\pm$ for the various benchmark points listed in Table 3 in the $\sin(\beta-\alpha) - \tan\beta$ plane. For BP1 with $(m_{H^\pm}, m_A, m_{h^0}, m_{H^0})$=(200, 50, 126, 700) GeV in panel (a), BR($H^\pm \to AW^\pm$) is independent of $\sin(\beta-\alpha)$, while decreasing at both large and very small $\tan\beta$, due to the competition of $H^\pm \to tb$ mode. BR($H^\pm \to AW^\pm$) can reach 90% or larger in the range $3 \lesssim \tan\beta \lesssim 15$. Even for $\tan\beta = 45$, BR($H^\pm \to AW^\pm$) can be around 50%.

For BP2 with $(m_{H^\pm}, m_A, m_{h^0}, m_{H^0})$=(300, 126, 126, 700) GeV in panel (b), BR($H^\pm \to AW^\pm$) decreases at small $|\sin(\beta-\alpha)|$ due to the opening of the $H^\pm \to h^0W^\pm$ channel. BR($H^\pm \to AW^\pm$) is maximized for $\sin(\beta-\alpha) = \pm 1$ and intermediate $\tan\beta$, which is also the preferred region in the h^0-126 case.

For BP3 with $(m_{H^\pm}, m_A, m_{h^0}, m_{H^0})$=(300, 700, 50, 126) GeV in panel (c), maximal branching fraction for $H^\pm \to h^0W^\pm$ is obtained around $\sin(\beta-\alpha) = 0$ where the coupling is maximal. The decreasing of the branching fraction at large and small $\tan\beta$ is caused by the enhanced tb and $\tau\nu$ modes, while the decreasing of the branching fraction at $\sin(\beta-\alpha) \sim \pm 1$ is caused by the suppressed $H^\pm \to h^0W^\pm$ decay width as well as the enhanced $H^\pm \to H^0W$ mode.

For BP4 with $(m_{H^\pm}, m_A, m_{h^0}, m_{H^0})$=(300, 700, 126, 700) GeV in panel (d), BR($H^\pm \to h^0W^\pm$) is suppressed at large $\tan\beta$ compared to BP3, since $H^\pm \to h^0W^\pm$ has more phase space suppression. The reduction of BR($H^\pm \to h^0W^\pm$) at larger $|\sin(\beta-\alpha)|$, however, is milder since $H^\pm \to H^0W^\pm$ is kinematically forbidden. In the preferred regions $\sin(\beta-\alpha) \sim \pm 1$ and $0.55 < \sin(\beta-\alpha) < 0.9$ (for $1.5 < \tan\beta < 4$) in the h^0-126 case, BR($H^\pm \to h^0W^\pm$) is still large enough to allow sensitivity in this channel.

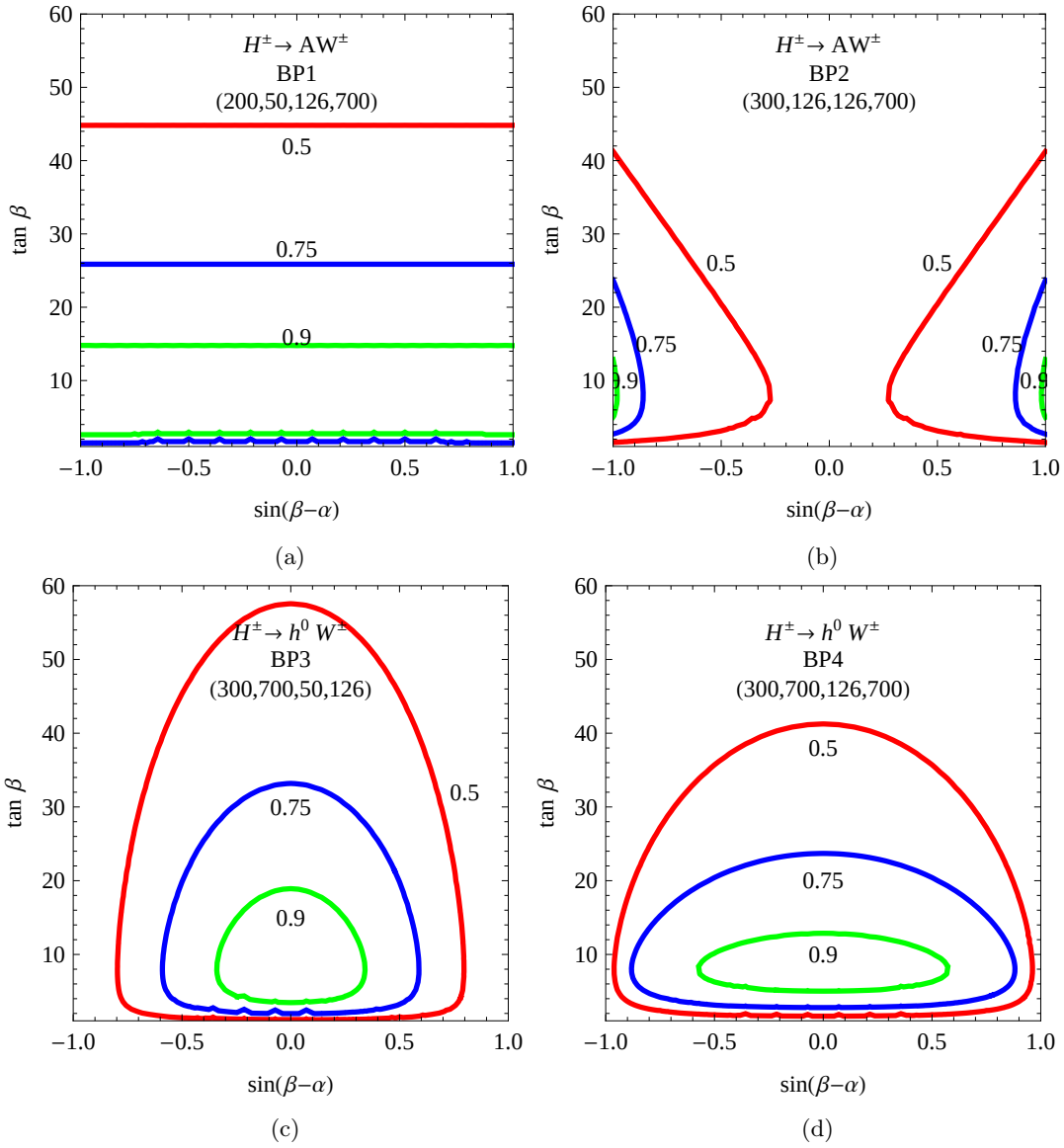

Figure 8. Contours of branching fractions of $H^\pm \to AW^\pm$ [(a) and (b)] and $H^\pm \to h^0 W^\pm$ [(c) and (d)] for each benchmark point.

5.2 Reach in parameter spaces

To translate the discovery and exclusion limits on $\sigma\times$BR in the $\tan\beta$ versus $\sin(\beta-\alpha)$ plane, we focus on the model implication for the $\tau\tau$ channel only since the limits for the bb channel are too weak to be realized within the Type II 2HDM.

In Fig. 9, we display the 95% exclusion (yellow regions enclosed by the solid lines) and 5σ discovery limits (cyan regions enclosed by the dashed lines) for the various benchmark points at the 14 TeV LHC with 300 fb^{-1} integrated luminosity. For BP1 with $H^\pm \to AW^\pm$ [panel (a)] , discovery is possible for small $\tan\beta \lesssim 1.5$ and for large $\tan\beta \gtrsim 45$, independent of $\sin(\beta-\alpha)$. The exclusion regions are much larger: $\tan\beta \lesssim 4$ and $\tan\beta \gtrsim 16$. Note that while the branching fraction is relatively suppressed at small and large $\tan\beta$, as shown in

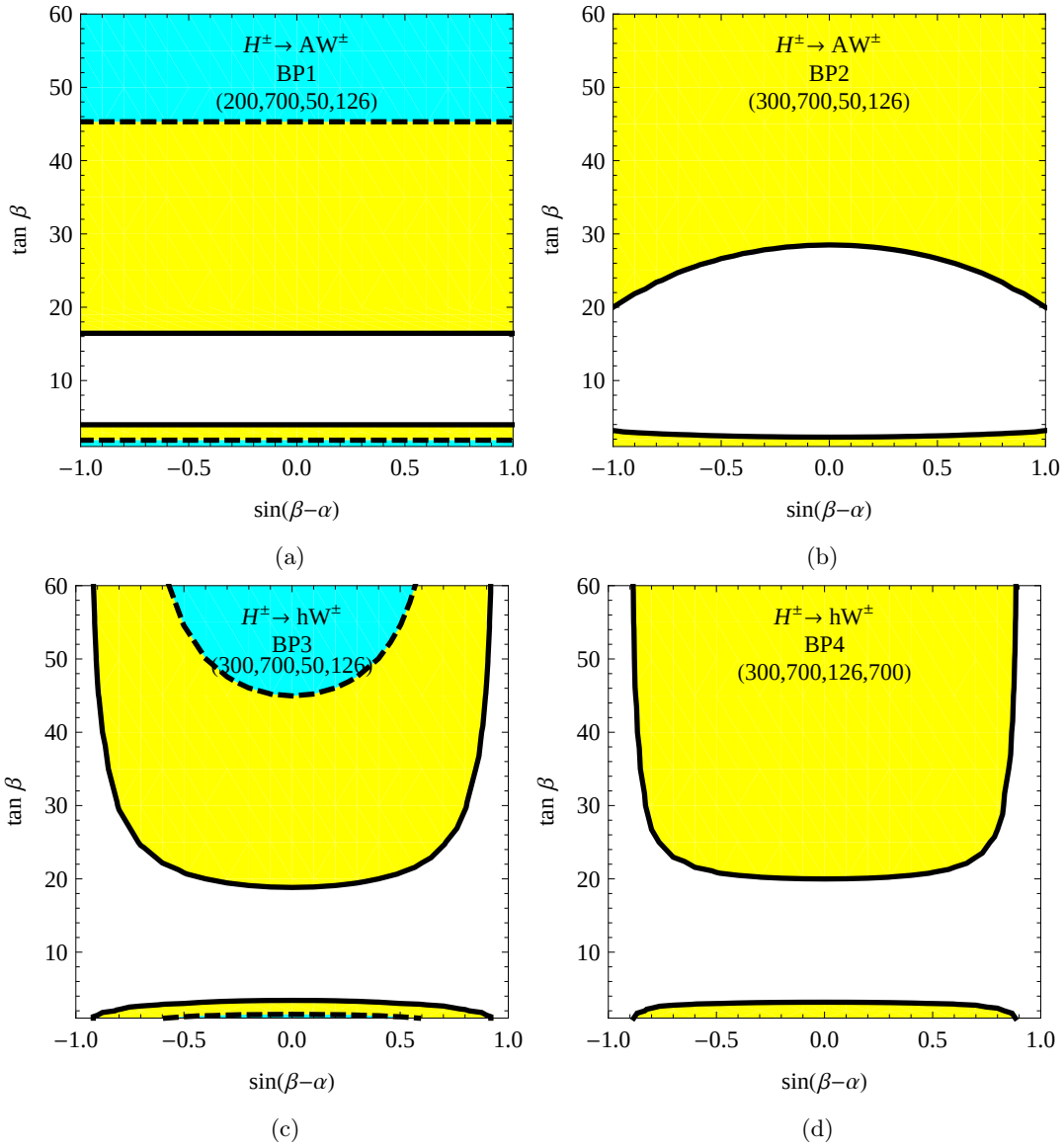

Figure 9. The 95% exclusion (yellow regions enclosed by the solid lines) and the 5σ discovery reach (cyan regions enclosed by the dashed lines) for $pp \to H^{\pm}tb \to AW^{\pm}tb/HW^{\pm}tb \to \tau\tau bbWW$ in the $\tan\beta$ versus $\sin(\beta-\alpha)$ plane for each benchmark point, with an integrated luminosity of 300 fb^{-1} at the 14 TeV LHC.

Fig. 8, the $H^{\pm}$ production cross section is enhanced in those regions, which are more than sufficient to offset the slightly reduced branching fractions. Therefore, we typically find exclusion and discovery regions appear in both the small and large $\tan\beta$ regions.

The reach for BP2 [panel (b)] is smaller compared to BP1 because of smaller cross sections associated with a 300 GeV $H^{\pm}$. The model could still be excluded in quite a large range: $\tan\beta \lesssim 3$, and $\tan\beta \gtrsim 20$. These values, however, are dependent on $\sin(\beta-\alpha)$. The maximum reach is achieved around $\sin(\beta-\alpha) = \pm 1$ where $\text{BR}(H^{\pm} \to AW^{\pm})$ is maximized. 5σ discovery, however, is not possible for this benchmark point.

For BP3 in panel (c), the reach is the best for $\sin(\beta-\alpha)=0$: $\tan\beta \gtrsim 20$ or $\lesssim 4$ for 95% C.L. exclusion and $\tan\beta \gtrsim 45$ or $\lesssim 1$ for 5σ discovery. The reach gets significantly weaker when $\sin(\beta-\alpha)$ approaches ± 1 with the regions $|\sin(\beta-\alpha)| > 0.8$ providing no reach. Note that for BP3 with $m_{H^0} = 126$ GeV, $\sin(\beta-\alpha) \approx 0$ is also the favored region given the SM-like Higgs consideration.

BP4 is an interesting case as this corresponds to the charged Higgs decaying to a SM-like Higgs h^0. The exclusion reach is almost the same as in BP3, while no discovery reach can be obtained due to the suppression of the branching fractions at large or small $\tan\beta$, as shown in Fig. 8 (d). Note that $H^\pm \to h^0 W^\pm$ is sensitive to part of the SM-like Higgs favored region: $0.55 < \sin(\beta-\alpha) < 0.9$ with small $\tan\beta$, with h^0 being SM-like.

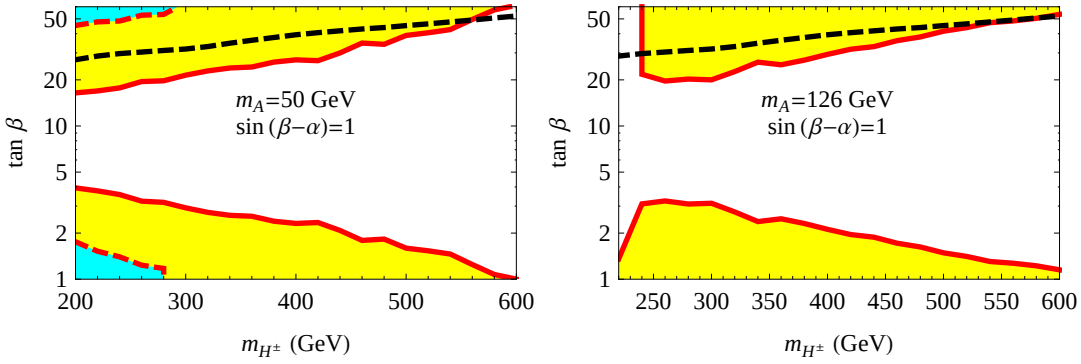

Figure 10. 95% exclusion (yellow regions bounded by solid red lines) and the 5σ discovery (cyan regions bounded by the dashed red lines) in the $m_{H^\pm} - \tan\beta$ parameter space for 300 fb^{-1} luminosity in the $pp \to H^\pm tb \to AW^\pm tb \to \tau\tau bbWW$ channel, with $m_A = 50$ GeV (left panel) and 126 GeV (right panel). Superimposed in black dashed line is the projected ATLAS $H^\pm \to \tau\nu$ 5σ discovery contours with 100 fb^{-1} luminosity. $\sin(\beta-\alpha)$ is chosen to be 1 and H^0 is decoupled.

Fig. 10 shows the reach in the $m_{H^\pm} - \tan\beta$ for $H^\pm \to AW^\pm$, with $m_A = 50$ GeV (left panel) and 126 GeV (right panel). We have fixed $\sin(\beta-\alpha) = 1$ and decoupled H^0 such that both $H^\pm \to h^0 W^\pm, H^0 W^\pm$ are absent. Superimposed on the plot in black dashed line is the projected ATLAS $H^\pm \to \tau\nu$ discovery reach with 100 fb^{-1} luminosity [30] for comparison. The $m_A = 50$ GeV represents the best case scenario for discovery/exclusion. While the reach in the exotic channel $H^\pm \to AW^\pm$ is smaller compared to the standard $H^\pm \to \tau\nu$ searches in the high $\tan\beta$ region, $AW^\pm$ channel provides a reach in the small $\tan\beta$ regions which is absent in the $\tau\nu$ mode. Additionally, the model can be excluded at the 95% C.L. for masses extending all the way to 600 GeV for both small and large $\tan\beta$ in this channel. The $m_A = 126$ case does not have sensitivity for discovery, but does provide an exclusion range that is comparable to the $m_A = 50$ GeV case.

We conclude this section with the following observations:

- The best case scenario are the decays $H^\pm \to AW^\pm$ for the h^0−126 case and $H^\pm \to h^0 W^\pm$ in the H^0−126 case for small daughter Higgs masses.
- The potentially interesting scenario $H^\pm \to h^0 W^\pm$ with h^0 being SM-like has sensitivity for 95% C.L. exclusion at small and large $\tan\beta$ for $\sin(\beta-\alpha)$ different from ± 1.

No sensitivity for discovery, however, can be obtained.

- There is sizeable reach in both small and large $\tan\beta$ for exclusion and discovery for $m_A = 50$ GeV and $\sin(\beta-\alpha) = 1$, as seen in Fig. 10. Discovery of the charged Higgs is possible for $m_{H^\pm}$ up to 280 GeV in both the small and large $\tan\beta$ regions.

- The reach in this exotic channel $H^\pm \to AW^\pm/HW^\pm$ is complementary to the conventional search channel $H^\pm \to \tau\nu$, in particular, for small $\tan\beta$.

6 Conclusion

The discovery of the Higgs at 126 GeV has not only confirmed the predictions of the SM, but has also ushered in a new era of discovery of beyond the SM physics. Many such scenarios incorporate an extended Higgs sector, which predict the existence of extra Higgs bosons other than the SM-like one. Most of the current searches for those extra Higgs bosons focus on the conventional channels of bb, $\tau\tau$, $\gamma\gamma$, WW and ZZ for the neutral ones, and $\tau\nu$, cs for the charged ones. However, there have been efforts recently to study the exotic decay of these Higgs bosons to enhance their collider reaches [36–38, 52–55].

Charged Higgses, compared to their neutral counterparts, are harder to discover. This is mostly due to the relatively small associated production cross section of $H^\pm tb$ (compared to the gluon fusion process for the neutral ones), as well as the large SM backgrounds for the dominant decay mode $H^\pm \to tb$. The conventional search channel $H^\pm \to \tau\nu$ suffers from relatively small decay branching fraction and thus, it behooves us to consider other possible decays of the $H^\pm$ to enhance its reach at colliders. In this paper, we analyzed the feasibility of discovering a charged Higgs boson in the process $H^\pm \to AW^\pm/HW^\pm$, with the daughter Higgs decaying to either $\tau\tau$ or bb.

We obtained model independent limits on $\sigma \times \mathrm{BR}(pp \to H^\pm tb \to AW^\pm tb/HW^\pm tb \to \tau\tau bbWW, bbbbWW)$ at the 14 TeV LHC. For the $\tau\tau$ channel, we considered all three cases: $\tau_{had}\tau_{had}$, $\tau_{lep}\tau_{had}$, and $\tau_{lep}\tau_{lep}$. It turns out that $\tau_{lep}\tau_{had}$ affords the best possible reach as we can take advantage of the same sign dilepton signal. Combining all three channels, we find for a daughter particle mass of 50 GeV, that the 95% C.L. exclusion reach ranges from about 70 fb to 25 fb, when $m_{H^\pm}$ is varied in the range 150 GeV−500 GeV with 300 fb^{-1} integrated luminosity at the 14 TeV LHC. The 5σ reach is about a factor of 3−4 higher. This channel is statistically limited and the reach enhances with increased luminosity. The reach in the bb channel is significantly worse.

We studied the implication of the $\sigma \times$ BR reach in the Type II 2HDM, focusing on $H^\pm \to AW^\pm$ and $H^\pm \to h^0 W^\pm$ decays. We find that in this model, the $pp \to H^\pm tb \to bbbbWW$ cross section is too low for $H^\pm$ to be either discovered or excluded. However, for the $\tau\tau$ mode, large regions of parameter space in $\tan\beta$ versus $\sin(\beta-\alpha)$ can be covered when the daughter Higgs mass is relatively light, in particular, for small and large $\tan\beta$. The exclusion region in the $m_{H^\pm} - \tan\beta$ plane can be extended to $m_{H^\pm} = 600$ GeV, while discovery is possible for $m_{H^\pm} \lesssim 280$ GeV. While the model can be excluded for a wide range of $\tan\beta$ values, discovery regions are mostly restricted to either small ($\lesssim 2$) or large ($\gtrsim 50$) values. Since the conventional search channel $H^\pm \to \tau\nu$ is only sensitive to the large

$\tan\beta$ region, the exotic decay mode $H^\pm \to AW^\pm/HW^\pm$ offers a complementary channel for charged Higgs searches.

Given the difficulties of the charged Higgs detection at hadron colliders, other search channels, for example, $qq' \to H^\pm$, electroweak pair production of H^+H^-, H^+W^-, as well as charged Higgs produced in the decay of a heavy Higgs [33, 35–38, 55, 56] should be studied to fully explore the discovery potential of the charged Higgses at the LHC. A future lepton machine with high center of mass energy would certainly be useful for charged Higgs discovery.

Acknowledgments

We thank Peter Loch, John Paul Chou, John Stupak and Martin Flechl for helpful discussions. We also wishes to acknowledge the hospitality of the Aspen Center for Physics where part of the work was finished. This work was supported by the Department of Energy under Grant DE-FG02-13ER41976.

References

[1] G. Aad *et al.* [ATLAS Collaboration], Phys. Lett. **B716** 1 (2012).

[2] G. Aad *et al.* [ATLAS Collaboration], ATLAS-CONF-2013-034.

[3] S. Chatrchyan *et al.* [CMS Collaboration], Phys.Lett. **B716** 30 (2012).

[4] S. Chatrchyan *et al.* [CMS Collaboration], CMS-PAS-HIG-13-005.

[5] G. Aad *et al.* [ATLAS Collaboration], Phys. Lett. B **726**, 120 (2013).

[6] G. C. Branco, P. M. Ferreira, L. Lavoura, M. N. Rebelo, M. Sher and J. P. Silva, Phys. Rept. **516**, 1 (2012).

[7] H.E. Haber, G.L. Kane and T. Sterling, Nucl. Phys. **B161**, 493 (1979).

[8] L.J. Hall and M.B. Wise, Nucl. Phys. **B187**, 397 (1981).

[9] J.F. Donoghue and L.F. Li, Phys. Rev. **D19**, 945 (1979).

[10] H. P. Nilles, Phys. Rept. **110**, 1 (1984).

[11] H. E. Haber and G. L. Kane, Phys. Rept. **117**, 75 (1985).

[12] R. Barbieri, Riv. Nuovo Cim. **11N4**, 1 (1988).

[13] J. R. Ellis, J. F. Gunion, H. E. Haber, L. Roszkowski and F. Zwirner, Phys. Rev. D **39**, 844 (1989).

[14] M. Drees, Int. J. Mod. Phys. A **4**, 3635 (1989).

[15] N. D. Christensen, T. Han, Z. Liu and S. Su, JHEP **1308**, 019 (2013); M. Drees, M. Guchait and D. P. Roy, Phys. Lett. B **471**, 39 (1999).

[16] B. Grinstein and P. Uttayarat, JHEP **1306**, 094 (2013) [Erratum-ibid. **1309**, 110 (2013)].

[17] C. -W. Chiang and K. Yagyu, JHEP **1307**, 160 (2013).

[18] B. Mohn, N. Gollub and K. A. Assamagan, ATL-PHYS-PUB-2005-017; K. A. Assamagan, Acta Phys. Polon. B **31**, 881 (2000).

[19] K. A. Assamagan, Y. Coadou and A. Deandrea, Eur. Phys. J. direct C **4**, 9 (2002).

[20] J. Beringer et al. (Particle Data Group), Phys. Rev. D86, 010001 (2012), and 2013 partial update for the 2014 edition;

[21] B. Coleppa, F. Kling and S. Su, JHEP **1401**, 161 (2014).

[22] F. Mahmoudi and O. Stal, Phys. Rev. D **81**, 035016 (2010).

[23] J. F. Gunion, H. E. Haber, G. L. Kane and S. Dawson, Front. Phys. **80**, 1 (2000).

[24] S. Moretti and W. J. Stirling, Phys. Lett. B **347**, 291 (1995) [Erratum-ibid. B **366**, 451 (1996)]; A. Djouadi, J. Kalinowski and P. M. Zerwas, Z. Phys. C **70**, 435 (1996).

[25] A. G. Akeroyd and S. Baek, Phys. Lett. B **525**, 315 (2002); A. G. Akeroyd, A. Arhrib and E. Naimi, Eur. Phys. J. C **20**, 51 (2001).

[26] G. Aad *et al.* [ATLAS Collaboration], JHEP **1303**, 076 (2013); G. Aad *et al.* [ATLAS Collaboration], JHEP **1206**, 039 (2012).

[27] G. Aad *et al.* [ATLAS Collaboration], ATLAS-CONF-2013-090.

[28] S. Chatrchyan *et al.* [CMS Collaboration], JHEP **1207**, 143 (2012); CMS-PAS-HIG-12-052.

[29] G. Aad *et al.* [ATLAS Collaboration], Eur. Phys. J. C **73**, 2465 (2013).

[30] Bjarte Mohn, Martin Flechl, and Johan Alwall, ATLAS-PHY-PUB-2007-006.

[31] R. Guedes, S. Moretti and R. Santos, JHEP **1210**, 119 (2012); M. Hashemi, JHEP **1305**, 112 (2013).

[32] M. Hashemi, Eur. Phys. J. C **72**, 1994 (2012).

[33] M. Hashemi, JHEP **1311**, 005 (2013).

[34] Q. -H. Cao, X. Wan, X. -p. Wang and S. -h. Zhu, Phys. Rev. D **87**, no. 5, 055022 (2013); S. Yang and Q. -S. Yan, JHEP **1202**, 074 (2012); K. A. Assamagan and N. Gollub, Eur. Phys. J. C **39S2**, 25 (2005).

[35] S. -S. Bao, X. Gong, H. -L. Li, S. -Y. Li and Z. -G. Si, Phys. Rev. D **85**, 075005 (2012).

[36] U. Maitra, B. Mukhopadhyaya, S. Nandi, S. K. Rai and A. Shivaji, Phys. Rev. D **89**, 055024 (2014).

[37] L. Basso, A. Lipniacka, F. Mahmoudi, S. Moretti, P. Osland, G. M. Pruna and M. Purmohammadi, JHEP **1211**, 011 (2012).

[38] R. Dermisek, J. P. Hall, E. Lunghi and S. Shin, arXiv:1311.7208 [hep-ph].

[39] V. Khachatryan *et al.* [CMS Collaboration], arXiv:1405.7570 [hep-ex].

[40] S. Dittmaier, M. Kramer, M. Spira and M. Walser, Phys. Rev. D **83**, 055005 (2011).

[41] B. Coleppa, F. Kling, A. Pyarelal and S. Su, "LHC reach for a light charged Higgs", to appear.

[42] J. Alwall, M. Herquet, F. Maltoni, O. Mattelaer and T. Stelzer, JHEP **1106**, 128 (2011); J. Alwall, R. Frederix, S. Frixione, V. Hirschi, F. Maltoni, O. Mattelaer, H. -S. Shao and T. Stelzer *et al.*, arXiv:1405.0301 [hep-ph].

[43] T. Sjostrand, S. Mrenna and P. Skands, JHEP **0605**, 026 (2006).

[44] S. Ovyn, X. Rouby and V. Lemaitre, arXiv:0903.2225 [hep-ph].

[45] A. Avetisyan *et. al.*, "Snowmass Energy Frontier Simulations for Hadron Colliders".

[46] http://www-ekp.physik.uni-karlsruhe.de/∼ott/theta/theta-auto/.

[47] G. Aad *et al.* [ATLAS Collaboration], Phys. Lett. B **717**, 330 (2012).

[48] N. Craig and S. Thomas, JHEP **1211**, 083 (2012).

[49] H. S. Cheon and S. K. Kang, JHEP **1309**, 085 (2013); A. Drozd, B. Grzadkowski, J. F. Gunion and Y. Jiang, JHEP **1305**, 072 (2013); S. Chang, S. K. Kang, J. -P. Lee, K. Y. Lee, S. C. Park and J. Song, JHEP **1305**, 075 (2013); C. -Y. Chen and S. Dawson, Phys. Rev. D **87**, no. 5, 055016 (2013).

[50] Martin Flechl, Michael Kramer, Sami Lehti, Sven Heinemeyer, https://twiki.cern.ch/twiki/bin/view/LHCPhysics/MSSMCharged.

[51] T. Hahn, S. Heinemeyer, W. Hollik, H. Rzehak and G. Weiglein, Phys. Rev. Lett. **112**, 141801 (2014); M. Frank, T. Hahn, S. Heinemeyer, W. Hollik, H. Rzehak and G. Weiglein, JHEP **0702**, 047 (2007); G. Degrassi, S. Heinemeyer, W. Hollik, P. Slavich and G. Weiglein, Eur. Phys. J. C **28**, 133 (2003); S. Heinemeyer, W. Hollik and G. Weiglein, Eur. Phys. J. C **9**, 343 (1999); S. Heinemeyer, W. Hollik and G. Weiglein, Comput. Phys. Commun. **124**, 76 (2000).

[52] B. Coleppa, F. Kling and S. Su, arXiv:1404.1922 [hep-ph]; Y. Amhis *et al.* [Heavy Flavor Averaging Group Collaboration], arXiv:1207.1158 [hep-ex], and online updates at http://www.slac.stanford.edu/xorg/hfag.

[53] E. Brownson, N. Craig, U. Heintz, G. Kukartsev, M. Narain, N. Parashar and J. Stupak, arXiv:1308.6334 [hep-ex].

[54] D. Curtin, R. Essig, S. Gori, P. Jaiswal, A. Katz, T. Liu, Z. Liu and D. McKeen *et al.*, arXiv:1312.4992 [hep-ph].

[55] L. Tong and S. Su, "Exotic Higgs Decay via Charged Higgs", in preparation.

[56] N. D. Christensen, T. Han and T. Li, Phys. Rev. D **86**, 074003 (2012).